Earth and Planetary Science Letters 478 (2017) 102–109

Contents lists available at ScienceDirect

Earth and Planetary Science Letters

www.elsevier.com/locate/epsl

The deep Peru 2015 doublet earthquakes

S. Ruiz [a,*], H. Tavera [b], P. Poli [c], C. Herrera [d], C. Flores [a,e], E. Rivera [a,e], R. Madariaga [f]

[a] Geophysics Department, Universidad de Chile, Chile
[b] Geophysical Institute of Peru, Lima, Peru
[c] Department of Earth, Atmospheric and Planetary Science, Massachusetts Institute of Technology, Cambridge, MA, USA
[d] School of Earth and Ocean Sciences, University of Victoria, Victoria, BC, Canada
[e] Geology Department, Universidad de Chile, Chile
[f] Laboratoire of Geologie, Ecole Normale Superieure, Paris, France

ARTICLE INFO

Article history:
Received 19 May 2017
Received in revised form 25 August 2017
Accepted 27 August 2017
Available online 17 September 2017
Editor: P. Shearer

Keywords:
deep earthquake
seismic source
kinematic inversion

ABSTRACT

On 24 November 2015 two events of magnitude Mw 7.5 and Mw 7.6 occurred at 600 km depth under the Peru–Brazil boundary. These two events were separated in time by 300 s. Deep event doublets occur often under South America. The characteristics that control these events and the dynamic interaction between them are an unresolved problem. We used teleseismic and regional data, situated above the doublet, to perform source inversion in order to characterize their ruptures. The overall resemblance between these two events suggests that they share similar rupture process. They are not identical but occur on the same fault surface dipping westward. Using a P-wave stripping and stretching method we determine rupture speed of 2.25 km/s. From regional body wave inversion we find that stress drop is similar for both events, they differ by a factor of two. The similarity in geometry, rupture velocity, stress drop and radiated energy, suggests that these two events looked like simple elliptical ruptures that propagated like classical sub-shear brittle cracks.

1. Introduction

On 24 November 2015 two large earthquakes of magnitudes Mw 7.5 and 7.6 occurred at 22:45:38 (UTC) and 22:50:54 (UTC) under the Peru–Brazil boundary between 9°S and 11°S inside a band between 600 and 700 km depth. Fig. 1 shows the epicenters of the November 2015 doublet and that of other large magnitude deep events that have occurred under South America: 1994 Bolivia Mw 8.2 (Kikuchi and Kanamori, 1994; Kirby et al., 1995) and 1970 Colombia Mw 8.0 (Furumoto, 1977). The mechanism of generation of these deep earthquakes is still unclear (Frohlich, 2006; Houston, 2015). Under the pressure and temperature condition of hundreds of kilometers deep into the mantle, plastic flow should be favored rather than brittle failure. Yet deep events on subducting tectonic plates are observed as shear rupture on faults, just as crustal earthquakes. Seismological observations show that deep events are characterized by certain properties that are different from shallower events: Radiated seismic energies (Wiens, 2001), *b*-values and aftershock sequences (Wiens and Gilbert, 1996; Frohlich, 2006; Houston, 2015; Zhan, 2017), source durations and stress drops (Campus and Das, 2000; Frohlich, 2006; Poli and Prieto, 2014, 2016).

Deep event doublets frequently occur in South America where several Mw ~7.0 events occurred clustered in time and space 1921–1922, 1961–1963, 1989–1990 and 2002–2003 (Okal and Bina, 1994; Ye et al., 2016). Using teleseismic data, Ye et al. (2016) proposed that the two events of 2015 had diverse rupture processes although they are closely located on the same fault structure. According to their study, the second event (E2) had a smaller rupture area and lower rupture velocity than the first event (E1). Zahradník et al. (2017) modeled regional waveforms for these events and observed close similarities in the total duration of both events and smaller rupture velocities than those proposed by Ye et al. (2016). Here, we determine the seismic source properties of these earthquakes using data obtained from regional networks, see Fig. 2, as well as teleseismic recordings. We also used the broad band regional data of the Peruvian and Brazilian networks to relocate the aftershocks of the doublet. We performed regional kinematic inversions for both events considering an elliptical source for both of them (Ruiz and Madariaga, 2013; Madariaga and Ruiz, 2016; Herrera et al., 2017). We obtain the rupture geometry, rupture velocity and the slip distribution of both events and we discuss the close similarity between them.

* Corresponding author.
E-mail address: sruiz@dgf.uchile.cl (S. Ruiz).

http://dx.doi.org/10.1016/j.epsl.2017.08.036
0012-821X/

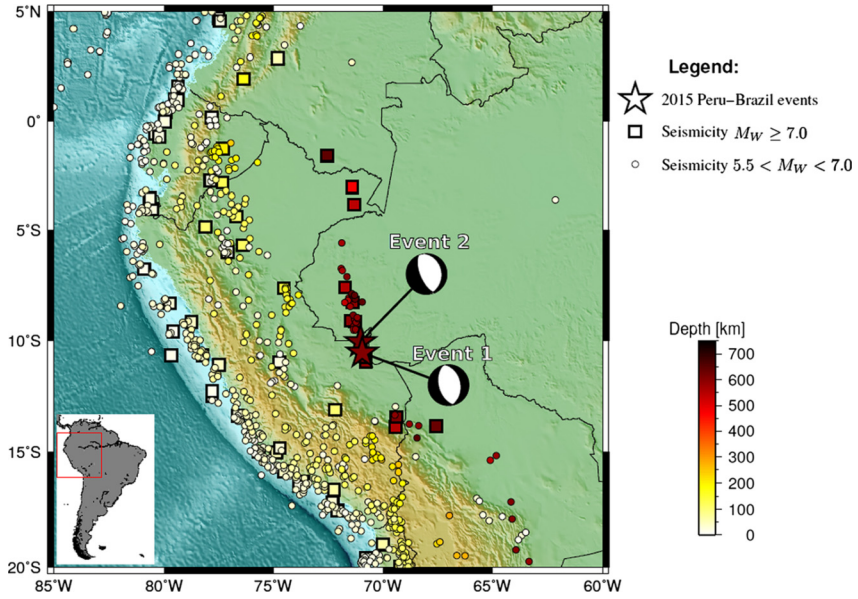

Fig. 1. Seismicity of South America since 1900 for events of magnitude larger than M 5.5 from the NEIC catalog. Squares denote events of magnitude larger than M 7.0. The stars denote the epicenters of the two events in the doublet of November 2015. The focal mechanism corresponds to the deep event doublet (USGS, National Earthquake Information Center, PDE).

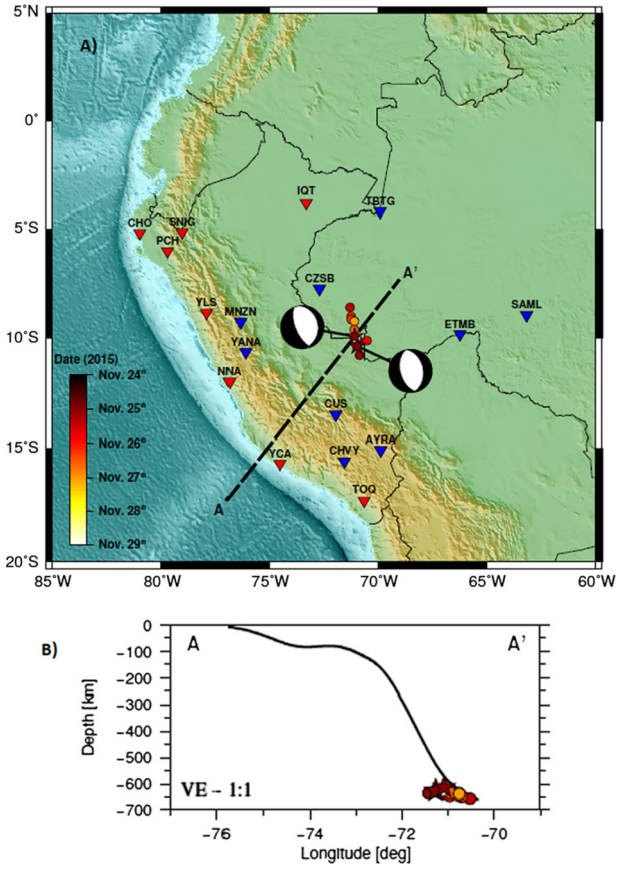

Fig. 2. Regional seismic data used to study the 2015 doublet in Peru. A) Inverted triangles denote the regional broad band instruments of the Peruvian and Brazilian seismic networks. The blue inverted triangles were used in the kinematic inversion and all of them were used to compute the localization of aftershocks. Dots are the aftershocks localized in this work. B) Vertical cross section along profile AA shown in panel A. Dots are the aftershocks of the Peru deep doublet, stars the hypocenter of the two main-shocks. The continuous line is the slab modeled by Hayes et al. (2012). The focal mechanisms are those of the two events in the 2015 doublet (USGS, National Earthquake Information Center, PDE). (For interpretation of the references to color in this figure legend, the reader is referred to the web version of this article.)

2. Data, methodology and results

The location of the two deep Peruvian events is shown in Figs. 1 and 2 as well as the local stations used to do body wave inversion. Throughout the paper we used the fault plane solutions proposed by USGS. Event E1 had a main fault plane with strike = 165, dip = 50, rake = −94 and event E2 had a fault plane with strike = 157, dip = 64, rake = −98 (USGS focal mechanism). Ye et al. (2016) and Zahradník et al. (2017) proposed slightly different mechanisms determined with either W-phase or moment tensor methods. As we will show the most likely rupture plane is the West dipping fault plane with dip of 50° (event E1) or 64° (event E2).

2.1. Teleseismic data and methodology

We use broadband seismic data for all the stations available at the time of the earthquakes. After deconvolution of the instrumental response we obtained velocity waveforms. We then analyzed the P waves in a frequency range from 0.01 to 2 Hz, ensuring that the signal to noise ratio (SNR) for each trace was larger than 10. The SNR is evaluated by comparing the maximum amplitude in 10 s window after the P wave arrival, with the mean absolute noise level in a similar window before the P wave arrival. We align the traces as explained by Poli and Prieto (2014) and Poli et al. (2016) to build an average source time function, from which approximate rupture duration is measured. The aligned data are then re-sampled in space using takeoff and azimuth grid of 10°, to avoid dominant azimuths in the inversion. Only data from 0° to 8° and from 32° to 88° distance were retained. We thus ensure that both down-going and up-going P waves are observed as they are needed to resolve the depth of the rupture (Kiser et al., 2011). Each signal is windowed from 5 s before the P waves to twice the estimated rupture duration.

We use the method of Warren and Silver (2006) to evaluate the source geometry and rupture velocity. This approach has been successfully applied to resolve the fault plane of different earthquakes from subduction zones and deep continental zones (Prieto et al., 2017). For each couple of waveforms we measure the stretching factor and the associated correlation coefficient. We retain all data with correlation larger than 0.9 after stretching. For each value of

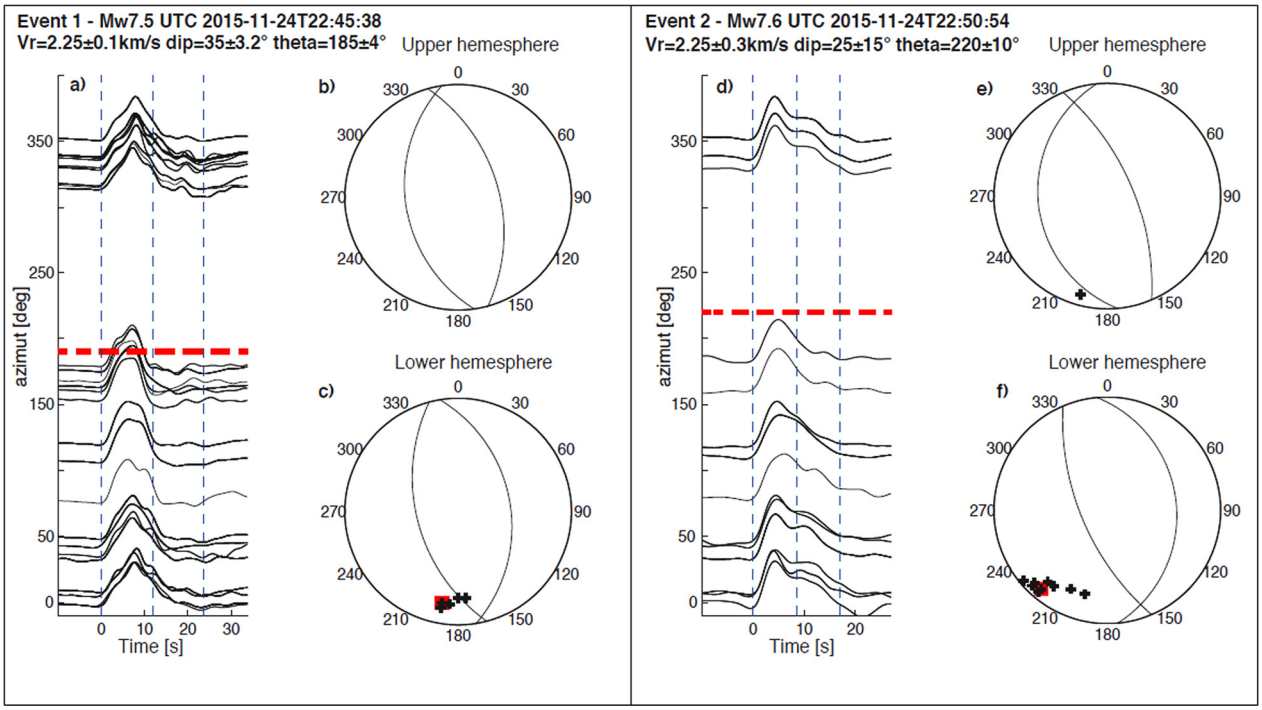

Fig. 3. Rupture properties for the two deep events of 2015. P waves are arranged as a function of azimuth, the red dashed line indicates the direction of the rupture. The focal mechanisms (upper and lower hemisphere) are also plotted, together with bootstrap (black crosses) and best (red square) solutions. The rupture parameters for each event are reported on the figure. Mechanisms are plotted with an equal angle projection (Wulf's net) in order to emphasize the good agreement between the angle of maximum directivity and the fault planes. (For interpretation of the references to color in this figure legend, the reader is referred to the web version of this article.)

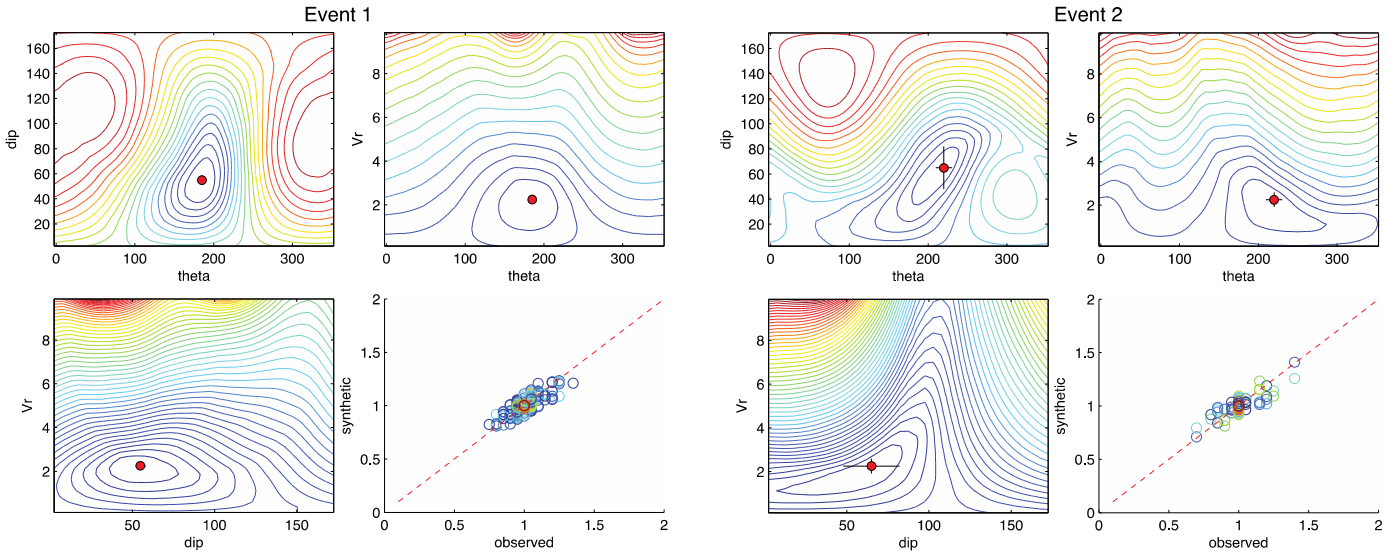

Fig. 4. Misfit surfaces as a function of rupture velocity, dip and rupture direction theta obtained from the grid search of the best solution for the two events. The bottom right plots for each event show the relationship between synthetic and observed stretching. The color is proportional to the correlation coefficients after stretching for each measurement (the lowest correlation is 0.97).

rupture velocity (Vr), rupture dip and rupture azimuth we calculated synthetic stretching, and compare them with observations. The grid search is repeated 100 times, and we randomly remove one of the high correlation measures each time. The result is stored every time, and the ensemble of the measures is used to evaluate the uncertainty of the estimates.

2.2. Teleseismic results

In Fig. 3 we plot the rupture properties of the two studied events. The first event (E1) has a rupture velocity of 2.25 km/s, and it suggests a rupture located on the west dipping fault plane of the focal mechanism (red square in Fig. 3c). The solution is well constrained as observed by the low scattering of the bootstrap results (black crosses in Fig. 3c). For the second event (E2) we also get a rupture velocity of 2.25 km/s. The larger scattering of the bootstrap solutions (black crosses in Fig. 3e–f) implies a less constrained rupture plane. However, the vicinity of the solutions with the west-dipping plane of the focal mechanism (Fig. 3f) suggests that the rupture is downward on this plane. A better assessment of the resolution is possible by studying the misfit isolines for the two events (Fig. 4). Clear minima are observed in all the plots in Fig. 4, illustrating the robustness of our estimates. The comparison

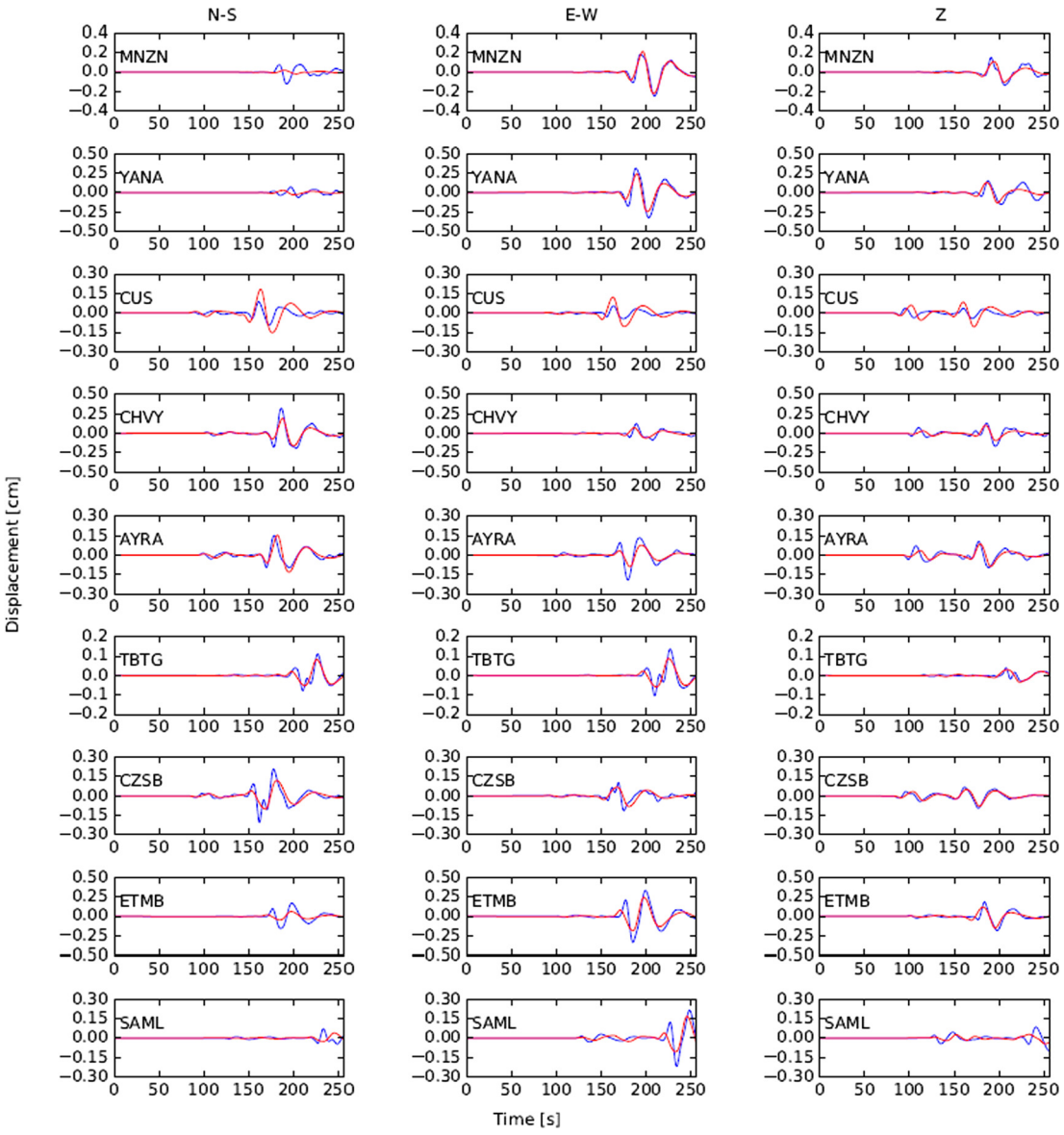

Fig. 5. Event E1 of the Peru doublet of 2015. Comparison between observed (blue) and synthetic (red) seismograms for the best model obtained by kinematic inversion using the Neighborhood Algorithm. The three components of 9 broad band records shown in Fig. 2 were inverted for Event E1. (For interpretation of the references to color in this figure legend, the reader is referred to the web version of this article.)

of the best solution synthetics and the observed stretching values for both events shows a remarkable high quality fit (Fig. 4d–h). From the rupture direction and focal mechanism we can conclude that the two events occurred probably on the same fault, which is the west down dipping plane of the CMT solutions (Fig. 1). Our rupture velocities are lower than those proposed Ye et al. (2016, Fig. 5), who proposed 4.5 km/s and 3 km/s for E1 and E2, respectively.

2.3. Location of aftershocks

We used the seismological regional data shown in Fig. 2 to localize the aftershocks of the 2015 Peru deep earthquakes. We cut the traces considering the USGS aftershock catalog, and we manually picked the first arrival of P and S waves. We use the Hypo71 software (Lee and Lahr, 1975) with the IASPEI 91 velocity model to locate the events. The aftershock distribution had a North–South orientation for almost 200 km, but no particular space-time migration was observed (see Fig. 2). Unfortunately, the signal-to-noise ratio of aftershock data is not good enough to get better relative locations nor to discriminate on which fault plane occurred the rupture.

2.4. Regional kinematic inversion

We model the seismic source using the regional data and a representative crack rupture of elliptical contour, with a centered elliptical slip distribution. We consider a kinematic model described by 6 parameters (Ruiz and Madariaga, 2013; Herrera et al., 2017). Five of them are geometric parameters, which are the semi-axes a and b of the ellipse, the rotation angle of the ellipse α and the location $(x_0,\ y_0)$ of its center inside the fault plane and we use an a priori elliptical slip distribution where we inverted the maximum slip D_{max}. In the inversion we fixed the rupture velocity to 2.25 km/s, the value determined from teleseismic analysis. The stations considered in the kinematic inversion were the closest to the hypocenter, we checked that the location of stations had a good azimuthal distribution (see Fig. 2). The real and simulated

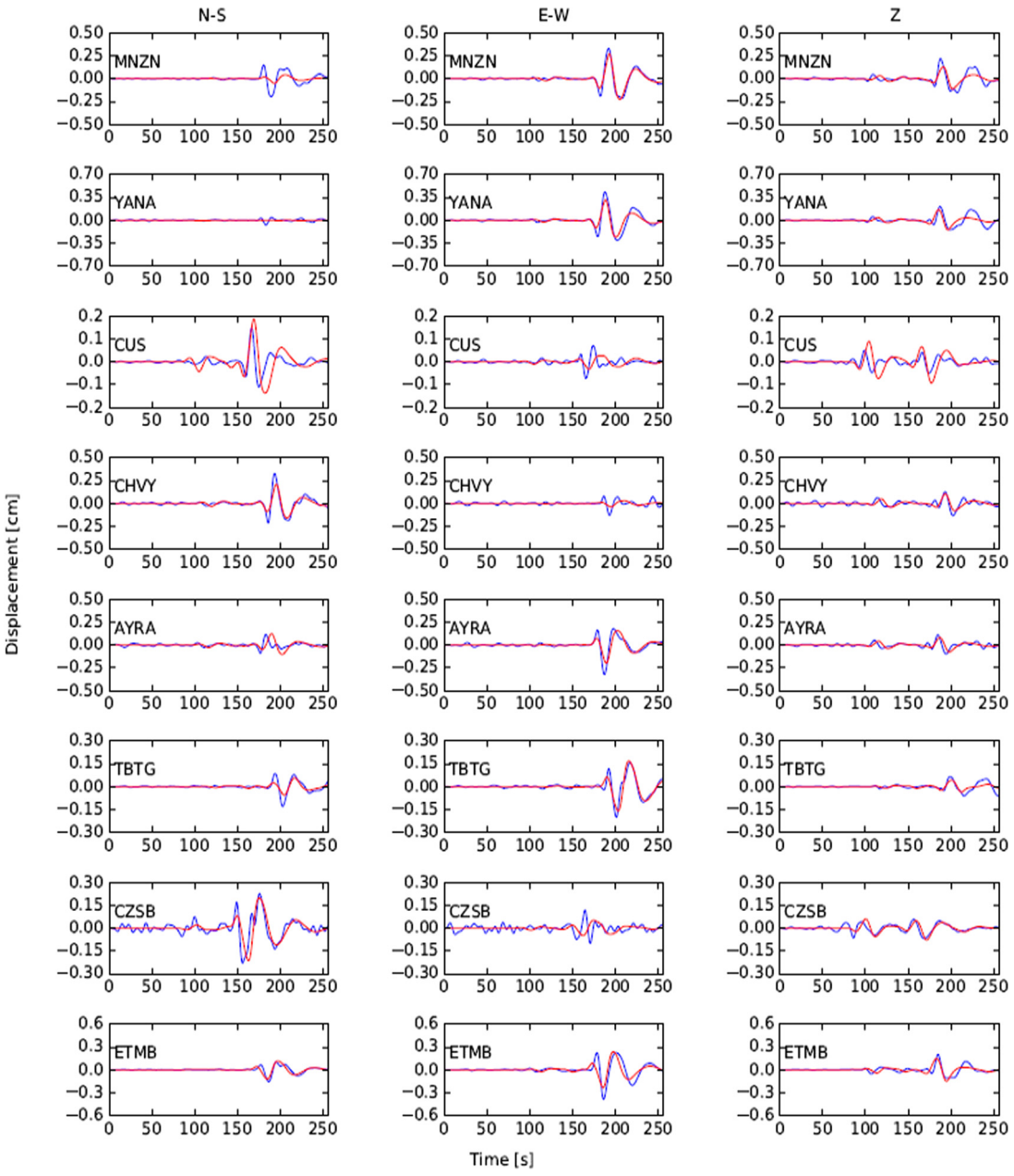

Fig. 6. Event E2 of the Peru doublet of 2015. Comparison between observed (blue) and synthetic (red) seismograms for the best model obtained by kinematic inversion using the Neighborhood Algorithm. The three components of the records of 8 of 9 broad band stations shown in Fig. 2 were inverted for the Event E2. The records of stations SAML was not inverted because the signal was affected by waves emitted by event E1. (For interpretation of the references to color in this figure legend, the reader is referred to the web version of this article.)

data were filtered in the same frequency band 0.02 Hz to 0.1 Hz. The kinematic inversion was made using the Neighborhood Algorithm in order to find the model that best fits the observed data. The fault planes for both events were discretized into a 30×30 grid of 50 km $\times$ 50 km, oriented with the strike, dip and rake related to the sub-vertical plane, in agreement with the fault plane obtained from teleseismic data and similar to the preferred fault plane of Ye et al. (2016) and Zahradník et al. (2017). We assumed an elliptical slip distribution inside the elliptical patch, similar to that a crack-like rupture (Madariaga and Ruiz, 2016).

The AXITRA code (Bouchon, 1981; Coutant, 1989) was used to simulate the wave propagation from the source to the receivers. We use a simplified velocity model defined in Table 1. The misfit χ^2 between observed and synthetic records generated for each of the tested models was calculated using the norm:

Table 1
Velocity model used to compute the Green functions.

Depth (km)	Vp (km/s)	Vs (km/s)	rho ($g\,cm^{-3}$)
0	6.0	3.46	2.70
33	8.1	4.40	3.30
200	9.2	5.00	3.30
350	10.24	5.91	4.07

$$\chi^2 = \frac{\sum_i (obs_i - synth_i)^2}{\sum_i obs_i^2} \quad (1)$$

where *obs* are the observed records and *synth* are the synthetics.

We generated 2860 models to obtain the best solutions of the events E1 and E2. The best solutions converge stably to a mini-

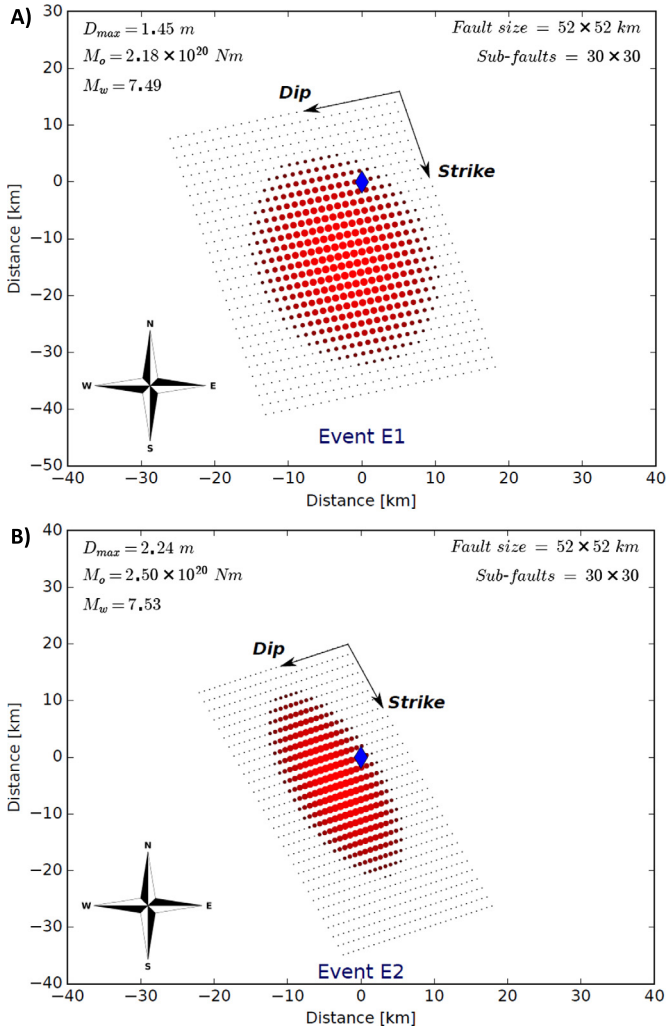

Fig. 7. Slip distribution of the deep Peru doublet of 2015. Slip distribution was determined using an elliptical patch geometry. A) Event E1 considering a fault plane with strike = 165, dip = 50, rake = −94. B) Event E2 considering a fault plane with strike = 157, dip = 64, rake = −98. Blue diamonds are the hypocenters, in these figures they correspond to point [0, 0]. (For interpretation of the references to color in this figure legend, the reader is referred to the web version of this article.)

mum misfit of $\chi^2 = 0.37$ for the first event and to $\chi^2 = 0.41$ for the second event. The comparison between the real and simulated traces is shown in Figs. 5 and 6 for events E1 and E2, respectively. Fig. 7 shows the slip distribution for both earthquakes. They have a similar elliptical rupture area of semi-axis 22.56 km and 22.42 km for E1 and 20.80 km and 17.99 km for E2. Event E2 had a maximum slip of 2.24 m and E1 had 1.45 m.

2.5. Spectra and waveforms of large Peru doublet

We computed the S wave Fourier spectra of the displacement records for the regional stations shown in Fig. 2. We removed the instrumental response, a linear trend, and then integrated once to get displacements from the broad-band records. Fig. 8A shows the ratio between the Fourier Spectra of events E2 and E1. The E2/E1 ratio is larger than 1 for long periods but is equal to 1 for higher frequencies. We observe in the regional data that the signals for the two events are remarkably similar both in the frequency and time domains. Fig. 8B shows the displacement spectra and the velocity waveforms for the two events recorded at the YCA station at a hypocentral distance of ∼700 km. Fig. 8B shows an almost similar S-wave corner frequency for both events (0.0623 and 0.0676 Hz, respectively), and the same can be observed directly from the duration of S waves for the all regional data. Thus we conclude that the two events were very similar, share the same fault plane and are contiguous in space.

3. Discussion

We have shown that the two deep Peruvian events of 2015 had very similar rupture geometries although the largest event (E2) had a smaller size by a factor of 1.2 (see Table 2). Let us first compare the dynamic properties and then we return to the similarity between the events. Since we used an elliptical crack model for the kinematic source we can compute the stress drop from the relations derived by Madariaga (1979). A very simple and accurate approximation is to compute stress drop approximating the rupture by a circular fault (Madariaga and Ruiz, 2016) using the average length of the two main axes of the rupture listed in Table 2. We obtain $\Delta\sigma = 8.4$ MPa and 15 MPa for events E1 and E2, respectively. Clearly event E2 has a higher stress drop than event E1 which is consistent with the larger seismic moment of E2 and its smaller size. We also computed stress drop from the teleseismic inversion. As shown in Table 2 stress drop range between 11.7 MPa and 12.8 MPa for events E1 and 11.6 MPa and 15.2 MPa for event E2. These values are somewhat different from those determined by Ye et al. (2016) who proposed stress drops of 2.3 MPa and 19.3 MPa for events E1 and E2, respectively.

We can now estimate radiated energy using Brune's model. The radiated fields by events E1 and E2 have the typical ω-squared spectral shape as can be verified in Fig. 8C. Thus we can use the ratio between radiated energy and strain energy drop for Brune's (1970) model:

$$E_R = 0.47\Delta U \tag{2}$$

(see Udias et al., 2014, eq. (9.40)). Strain energy release ΔU can be computed using the same circular crack approximation described above, so that

$$\Delta U = \frac{8\Delta\sigma^2}{7\mu}a^3 \tag{3}$$

where μ is the rigidity of the medium near the source depth. From (2) and (3) we obtain $E_R = 3.02 \times 10^{15}$ J for event E1 and $E_R = 6.20 \times 10^{15}$ J for E2. See also Table 2. It is possible to compute the radiated energy using the more accurate expression derived by Udias et al. (2014, eq. (9.41)) that does not assume the corner frequency radius relation by Brune (1970), but the values are actually very similar.

We compare these values for E_R and $\Delta\sigma$ with those of the teleseismic study (see Supplementary material). The radiated seismic energy is 4.7×10^{15} J and 6.9×10^{15} J for events E1 and E2, respectively. These results agree with our regional kinematic inversion, as shown in Table 2.

The stress drop and radiated energy estimates are in the expected range for deep earthquakes (Poli and Prieto, 2016; Herrera et al., 2017). These values are also in agreement with those proposed by Ye et al. (2016) who found $E_s = 4.2 \times 10^{15}$ J for E1 and 7.6×10^{15} J for E2. Thus we agree that radiated energy from E2 is about twice that radiated by E1. This is also consistent with the higher corner frequency determined for E2 in Fig. 8C.

In contrast to the results obtained by Ye et al. (2016), we propose similar rupture geometry and rupture velocity for both events. As shown in Fig. 8 the best available record of the two events in a Peruvian station shows practically the same spectrum, and almost the same source time function, although event 2 seems slightly shorter. The similarity of all estimated parameters implies

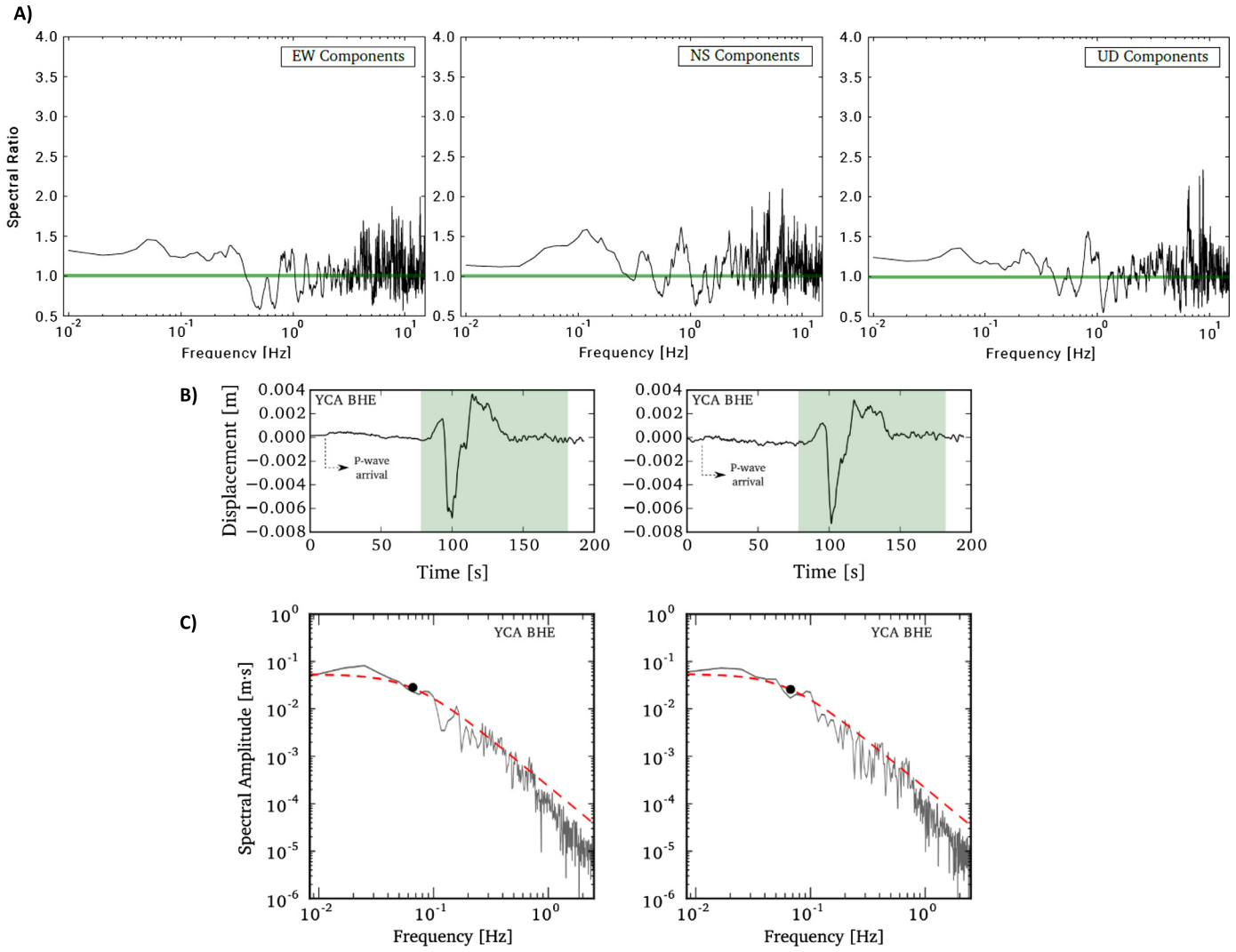

Fig. 8. A) Spectra of the 2015 deep Peruvian doublet. Spectral ratio between the spectra of events E2 and E1 obtained using a 10-point mobile window of the S wave Fourier spectra. The spectrum correspond to the average of the spectra recorded by stations shown in Fig. 2, the spectra were corrected only by the hypocentral distance. B) and C) Comparison of spectra and velocity waveform for E1 (left figure) and E2 (right figure). B) Displacement record at the YCA station (Fig. 2), the time series were corrected for instrument response, we remove a linear trend and integrated once. No filter was applied. C) The Fourier Spectrum was evaluated on the S wave window (gray zone in the time series). The hypocentral distance of event E1 form YCA was 687 km and 727 km for event E2. Corner frequencies, shown by a dot in the spectrum, are 0.0623 Hz and 0.0676 Hz for events E1 and E2, respectively.

Table 2
Parameters obtained from kinematic regional inversion and teleseismic inversion.

Event	Kinematic regional inversion				Teleseismic inversion	
	Mo (Nm)	Semi-axis (km)	Stress drop (MPa)	Radiated energy (J)	Stress drop (MPa)	Radiated energy (J)
E1	2.18e20	$a = 22.56/b = 22.42$	8.4	3.02e15	11.7–12.8	4.70e15
E2	2.50e20	$a = 20.80/b = 17.99$	15	6.20e15	11.6–15.2	6.90e15

a similar dynamic rupture for these two events, which suggests that they probably nucleated under similar pressure and temperature conditions. Furthermore, considering that E2 is larger than E1, the smaller energy released by the latter agree with a constant energy moment ratio, Er/Mo, which are 2.1×10^{-5} and 2.7×10^{-5} for events E1 and E2 respectively. These are also very similar to those determined by Ye et al. (2016).

Finally, why did Ye et al. (2016) propose that the two events were significantly diverse? For the first event E1 our results are very similar to theirs, while for event E2 they are quite different. Although the moments are very similar for event E2, their slip distribution has an equivalent radius of only a few km. We believe that this may be due to the selection of data or smoothing for the inversion of the slip function. We also found that many far field records were very noisy. Actually, the deconvolved P waves shown in Fig. 3 show the strong similarity between the two events. As these authors note, it is possible that the back-projection method does not see the whole fault.

4. Conclusions

We determined seismic rupture parameters for the two main events of the deep earthquake doublet that occurred in the Pe-

ruvian slab in November 2015. These events are exceptional as they occur 5 min apart at depth >600 km. The analysis of focal mechanisms, together with the similarity of both ruptures areas shown in Table 2, indicate that the two events occurred on basically the same fault. Furthermore, using P wave deconvolution (Figs. 3 and 4) we determined these events share similar rupture velocity of about 2.25 km. We assumed a crack-like slip distribution in the kinematic inversion, and then we derived stress drop and seismic energy which are in rough agreement with those determined by previous authors (Ye et al., 2016; Zahradník et al., 2017). The overall resemblance between these two events suggests that they share similar rupture mechanism. The similarity in geometry, rupture velocity, stress drop and radiated energy, suggests that these events nucleated under very similar conditions, although event E2 has a smaller length for a slightly larger moment.

Acknowledgements

We thank the Incorporated Research Institutions for Seismology Data Management Center, the Peruvian Seismic Network and the Seismological Center at the University of São Paulo, USP, Brazil, who provided the data used in this work. We thank the support of the Programa Riesgo Sísmico (AIN, Universidad de Chile) and FONDECYT project Number 1170430.

Appendix A. Supplementary material

Supplementary material related to this article can be found online at http://dx.doi.org/10.1016/j.epsl.2017.08.036.

References

Bouchon, M., 1981. A simple method to calculate Green's functions for elastic layered media. Bull. Seismol. Soc. Am. 71 (4), 959–971.
Brune, J., 1970. Tectonic stress and the spectra of seismic shear waves from earthquakes. J. Geophys. Res. 75, 4997–5009.
Campus, P., Das, S., 2000. Comparison of the rupture and radiation characteristics of intermediate and deep earthquakes. J. Geophys. Res. 105, 6177–6189. http://dx.doi.org/10.1029/1999JB900384.
Coutant, O., 1989. Programme de simulation numérique AXITRA. Res. Report LGIT, Grenoble, France.
Frohlich, C., 2006. Deep Earthquakes. Cambridge Univ. Press, Cambridge.
Furumoto, M., 1977. Spatio-temporal history of the deep Colombia earthquake of 1970. Phys. Earth Planet. Inter. 15, 1–12.
Hayes, G.P., Wald, D.J., Johnson, R.L., 2012. Slab1.0: a three-dimensional model of global subduction zone geometries. J. Geophys. Res. 117, B01302. http://dx.doi.org/10.1029/2011JB008524.
Herrera, C., Ruiz, S., Madariaga, R., Poli, P., 2017. Dynamic inversion of the 2015 Jujuy earthquake and similarity with other intraslab events. Geophys. J. Int. 209, 866–875.
Houston, H., 2015. Treatise on Geophysics, vol. 4, Earthquake Seismology, 2nd ed. Elsevier, Amsterdam, pp. 329–354.
Kikuchi, M., Kanamori, H., 1994. The mechanism of the deep Bolivia earthquake of June 9, 1994. Geophys. Res. Lett. 21, 2341–2344.
Kirby, S., Okal, E., Engdahl, R., 1995. The 9 June 94 Bolivian deep earthquake: an exceptional event in an extraordinary subduction zone. Geophys. Res. Lett. 22, 2233–2236.
Kiser, E., Ishii, M., Langmuir, C.H., Shearer, P.M., Hirose, H., 2011. Insights into the mechanism of intermediate-depth earthquakes from source properties as imaged by back projection of multiple seismic phases. J. Geophys. Res. B 116, B06310.
Lee, W.H.K., Lahr, J.C., 1975. HYP071 (Revised): A Computer Program for Determining Hypocenter, Magnitude, and First Motion Pattern of Local Earthquakes. U.S. Geological Survey Open File Report 75-311, 113 pp.
Madariaga, R., 1979. On the relation between seismic moment and stress drop in the presence of stress and strength heterogeneity. J. Geophys. Res. 84, 2242–2250.
Madariaga, R., Ruiz, S., 2016. Earthquake dynamics on circular faults: a review 1970–2015. J. Seismol. 20, 1059–1073.
Okal, E.A., Bina, C.R., 1994. The deep earthquakes of 1921–1922 in northern Peru. Phys. Earth Planet. Inter. 87, 33–54.
Poli, P., Prieto, G., 2014. Global and along-strike variations of source duration and scaling for intermediate-depth and deep-focus earthquakes. Geophys. Res. Lett. 41, 8315–8324.
Poli, P., Prieto, G., 2016. Global rupture parameters for deep and intermediate-depth earthquakes. J. Geophys. Res. B 121, 8871–8887.
Poli, P., Prieto, G., Rivera, E., Ruiz, S., 2016. Earthquakes nucleation and thermal shear instability in the Hindu-Kush intermediate-depth nest. Geophys. Res. Lett. 43, 1537–1542.
Prieto, G.A., Froment, B., Yu, C., Poli, P., Abercrombie, R., 2017. Earthquake rupture below the brittle–ductile transition in continental lithospheric mantle. Sci. Adv. 3, e1602642.
Ruiz, S., Madariaga, R., 2013. Kinematic and dynamic inversion of the 2008 Northern Iwate earthquake. Bull. Seismol. Soc. Am. 103, 694–708.
Udias, A., Madariaga, R., Buforn, E., 2014. Source Mechanisms of Earthquakes, Theory and Practice. Cambridge University Press, Cambridge, UK.
Warren, L., Silver, P., 2006. Measurement of differential rupture durations as constraints on the source finiteness of deep-focus earthquakes. J. Geophys. Res. B 11.
Wiens, D.A., 2001. Seismological constraints on the mechanism of deep earthquakes: temperature dependence of deep earthquake source properties. Phys. Earth Planet. Inter. 127, 145–163.
Wiens, D.A., Gilbert, H.J., 1996. Slab temperature effects on deep earthquake aftershock productivity and magnitude–frequency relations. Nature 384, 153–156.
Ye, L., Lay, T., Kanamori, H., Zhan, Z., Duputel, Z., 2016. Diverse rupture processes in the 2015 Peru deep earthquake doublet. Sci. Adv. 2, e1600581.
Zahradník, J., Čížková, H., Bina, C.R., Sokos, E., Janský, J., Tavera, H., Carvalho, J., 2017. A recent deep earthquake doublet in light of long-term evolution of Nazca subduction. Sci. Rep. 7, 45153. http://dx.doi.org/10.1038/srep45153.
Zhan, Z., 2017. Gutenberg–Richter law for deep earthquakes revisited: a dual-mechanism hypothesis. Earth Planet. Sci. Lett. 461, 1–7.